Chemical weathering variability during last glacial-interglacial cycle: A geochemical study of Bay of Bengal sediments

A Thesis
submitted in partial fulfilment of the requirements for the M.Sc. Degree Programme

by

Kankan Roy

20236403

Indian Institute of Science Education and Research

Pune - 411008, Maharashtra, India

April 17, 2025

under the guidance of

Dr. Gyana Ranjan Tripathy

Department of Earth and Climate Science

IISER Pune

Certificate

This is to certify that this dissertation entitled **Chemical weathering variability during last glacial-interglacial cycle: A geochemical study of Bay of Bengal sediments** towards the partial fulfilment of the M.Sc. Geology degree programme at the Indian Institute of Science Education and Research, Pune represents study/work carried out by **Kankan Roy** at IISER Pune under the supervision of **Dr. Gyana Ranjan Tripathy**, Associate Professor, Department of Earth and Climate Science, during the academic year 2024-2025.

Kankan Roy
(M.Sc. Student)

Dr. Gyana Ranjan Tripathy
(Supervisor)

This thesis is dedicated to my family and friends, and to all my well-wishers for their constant support and encouragement throughout this journey

Declaration

I hereby declare that the research work presented in the report entitled **Chemical weathering variability during last glacial-interglacial cycle: A geochemical study of Bay of Bengal sediments** have been carried out by me at the Department of Earth and Climate Science, Indian Institute of Science Education and Research, Pune under the supervision of Dr. Gyana Ranjan Tripathy and the same has not been submitted elsewhere for any degree.

Kankan Roy
(M.Sc. Student)

Dr. Gyana Ranjan Tripathy
(Supervisor)

ACKNOWLEDGEMENTS

I would like to take this opportunity to express my heartfelt appreciation to all those who have contributed to the successful completion of my dissertation at IISER Pune.

To begin with, I am immensely thankful to my supervisor, Dr. Gyana Ranjan Tripathy, for his insightful mentorship and unwavering encouragement throughout the course of this work. His profound knowledge and critical guidance played a vital role in developing my ideas and enhancing the overall quality of this thesis.

I would also like to sincerely thank my thesis expert, Dr. Sudipta Sarkar, for his valuable suggestions and constructive feedback during my mid-term evaluation. His input not only deepened my understanding of the subject but also helped me refine key aspects of my research.

My gratitude extends to the LDEO core repository for providing access to the sediment core VM29-19PC, which formed the foundation of this study. A portion of the experimental work presented here was carried out using the XRF facility at IISER Pune, funded through support from the DST-FIST program, and I gratefully acknowledge this assistance.

I am especially thankful to Kruttika Mohapatra, my mentor and lab mate, whose constant support, dedication, and willingness to share her expertise were crucial in the timely and successful execution of this project. Her encouragement and guidance were truly invaluable. I am also deeply appreciative of my fellow lab members Rakesh Kumar Rout and Achyuth Venugopal, whose camaraderie, collaborative spirit, and scientific inputs created a nurturing and productive research environment within the GRASP Lab.

I extend my special thanks to Shuvashree Maity, Vikrant Bartakke, and Vibhas Shevde for their consistent help, technical assistance, and enthusiastic support throughout this work. Their contributions, both big and small, have made a lasting impact on my journey.

I would also like to acknowledge my other lab mates, Akashi Baruah, Debasish Maji, Vaishali Bamrara and express heartfelt thanks to my friend and batchmate Nitin Panwar, whose constant motivation and positivity have been a source of strength. Last but not least, I am incredibly grateful to my family for their unconditional support, encouragement, and patience, which have sustained me through every stage of this academic pursuit.

Contents

List of Figures

List of Tables

ABSTRACT

Continental weathering and sediment transport are strongly influenced by climatic fluctuations. Studies from the Bay of Bengal, however, provide diverging evidence for the weathering and climate coupling. In this study, we present high-resolution major oxides concentration data for a sediment core VM29-19PC (water depth: 3182 m), retrieved from the western Bay of Bengal, to reconstruct variations in chemical weathering intensity and sediment provenance over the past ~35,000 years. The chronology of this core was established in an earlier study using AMS radiocarbon dating of planktic foraminifera, confirming a continuous sedimentary archive spanning the last glacial–interglacial cycle. Geochemical indices, particularly an increase in the Chemical Index of Alteration (CIA) and a concurrent decline in K/Al ratios, suggest progressive intensification of chemical weathering beginning around 25 ka, likely driven by climatic amelioration. These variations are synchronous with climatic transitions, and point to affect of enhanced monsoonal activity on continental weathering via increased continental runoff. The observed trends reflect a dynamic interplay between monsoon-driven hydrological shifts and regional erosion patterns, highlighting the sensitivity of weathering regimes to long-term climate variability in South Asia.

1 INTRODUCTION

1.1 Introduction

Chemical weathering and sediment transport are fundamental Earth surface processes that significantly influence topography, oceanic chemistry, and climate regulation over geologic timescales. Weathering refers to the breakdown of rocks through physical disintegration, chemical alteration, or biological activity, while erosion involves the transport of these weathered materials from their source regions to depositional environments. A range of factors—including tectonic setting, basin morphology, bedrock composition, climate variables (such as precipitation, temperature, and runoff), and vegetation cover—governs the intensity of weathering within fluvial systems. However, the influence of these controls is neither uniform across space nor consistent through time. On million-year timescales, for instance, chemical weathering of silicates driven by carbonic acid plays a key role in long-term atmospheric CO_2 drawdown (Raymo and Ruddiman, 1992). It has been proposed that the progressive uplift of the Himalayan-Tibetan Plateau intensified chemical weathering, thereby contributing to global cooling during the late Cenozoic (Raymo and Ruddiman, 1992; Richter et al., 1992). More recent perspectives emphasize that weathering may also release CO_2, particularly through oxidation of petrogenic organic carbon and sulfide minerals, which may in turn contribute to global warming scenarios (Hilton and West, 2020). On kilo-year timescales, the relationship between climate and erosion becomes more nuanced, with varying contributions from different climatic and geological drivers (Tripathy et al., 2014; Samanta et al., 2022). Furthermore, the climate-weathering interaction is modulated by whether the landscape operates under kinetic (reaction- rate) or supply (material-availability) limited weathering regimes (West et al., 2005).

The Himalayan region is recognized for its remarkably high rates of both physical erosion and chemical weathering, making it an ideal natural laboratory for examining past changes in erosion and related controlling factors (Milliman and Meade, 1983). The Himalayan Rivers transport substantial sediment loads into the Bay of Bengal (BoB), with the majority of this material being deposited along the basin's northern and western margins due to intense runoff (Goodbred and Kuehl, 1999, 2000; Milliman and Syvitski, 1992). Collectively, the Ganga and Brahmaputra rivers deliver approximately 1060 million tons of sediments annually to the BoB,

accounting for about 5% of the total global riverine sediment supply, despite draining only 1.3% of the Earth's land area (1.59 million km²; Milliman and Syvitski, 1992). Other prominent rivers contributing to the sediment budget of the BoB include the Godavari (170 million tons/year), Krishna (64 million tons/year), Mahanadi (60 million tons/year), and Irrawaddy (260 million tons/year) (Milliman and Syvitski, 1992).

There have been several studies on Himalayan erosion with respect to climate change which have documented diverging views. For example, geochemical and isotopic studies of the Ganga floodplain (Rahaman et al., 2009) and Bay of Bengal (Tripathy et al., 2011; 2014) sediments have shown reduction in sedimentary contribution from the Himalayas during the Last Glacial Maximum (LGM). The main reason for this reduction in sediment contribution is due to the decrease of the exposed surface area for weathering in the Himalayas and also the weakening of monsoon during LGM (Peketi et al., 2020). A similar study from the Arabian sea (Lupker et al., 2013) indicates intensification of chemical weathering during relatively warmer and wetter intervals of the Holocene compared to drier and cooler phases (Cai et al., 2019). This clearly explains the strong connection between weathering intensity and climate variability. In contrast, Sr-Nd isotopic study of sediments from the central Bay of Bengal (Galy et al., 2009) has shown a relatively stable erosion rates during climatic transitions. Similar isotopic study from the Arabian Sea (Goswami et al., 2012) has suggested effect of circulation pattern on relative sediment contribution from various sources. von Blanckenburg et al. (2015) have also found no major connection between climate and erosional intensity. Other studies have proposed the influence of various non-climatic driving forces, i.e. basin morphology, tectonic activity and lithology on erosion over millennial timescale (Mandal et al., 2015; White et al., 1999; Bluth and Kump, 1994). These differing inferences may be a result of varying locations, provenance characteristics and sediment transport pathways, which needs to be ascertained in future studies to pinpoint the weathering-climate interaction, if any, for the Himalayan river basins.

1.2 Objectives of the Thesis

The main objectives of the thesis are:

- To reconstruct past changes in the chemical weathering intensity during the last glacial-interglacial cycle using chemistry of Bay of Bengal sediments.
- To apportion the sedimentary sources to the western Bay of Bengal using ratios of immobile elements

- To establish the coupling between climate and weathering in the Himalayan region by comparing past climatic and our erosional record

1.3 Structure of the Thesis

The thesis is organized into four major sections, each addressing a specific component of the study:

- **Section 1** introduces the fundamental concepts of weathering and erosion, highlighting their long-term connection with climate variability across geological timescales. It reviews key existing literature.
- **Section 2** focuses on geological framework and oceanographic characteristics of the Bay of Bengal.
- **Section 3** details the methodologies adopted for geochemical analyses using the X-ray fluorescence (XRF) instrument. This section also outlines the accuracy and reproducibility of the geochemical measurements.
- **Section 4** includes the results generated by analytical methods
- **Section 5** focuses on the interpretation of these trends in the context of environmental and climatic processes.
- **Section 6** summarizes the main findings derived from the study, and the interpretations drawn from the results, thereby providing an integrated understanding of the research outcomes.

2 STUDY AREA: THE BAY OF BENGAL

Located in the northeastern sector of the Indian Ocean, the Bay of Bengal (BoB) is bounded by the Indian subcontinent to the west and northwest, Bangladesh to the north, and Myanmar along with the Andaman and Nicobar Islands to the east, as shown in Fig. 1. Several major rivers—including the Ganga, Brahmaputra, Mahanadi — discharge their waters into this basin. The total annual river runoff into the BoB is estimated to be around 2,950 km^3 (Sengupta et al., 2006), which accounts for over half of the freshwater input into the tropical Indian Ocean. As a result of this significant freshwater influx, the surface salinity in the BoB is considerably lower, with an average reduction of approximately 7‰ (Mohanty et al., 2008). In contrast, the Arabian Sea (AS), positioned in the north-western part of the Indian Ocean, exhibits higher salinity levels, largely due to intense evaporation in that region. This contrast in salinity between the BoB and AS is moderated through ocean circulation patterns. During the winter months, the East India Coastal Current (EICC), which flows southward, transports low- salinity surface waters from the northern BoB and transfers them to the West India Coastal Current (WICC), which then moves northward into the Arabian Sea.

The Indian Peninsula exhibits a diverse geological framework composed of multiple lithotectonic domains. These include: (i) the Archean cratonic regions of Dharwar, Bastar, Singhbhum, and Bundelkhand, which are characterized by the Peninsular Gneissic Complex comprising granitic gneisses, phyllites, schists, amphibolites, and tonalite-trondhjemite-granodiorite (TTG) assemblages; (ii) Proterozoic mobile belts such as the Eastern Ghats, Aravalli, Satpura, and the Southern Granulite Terrain, consisting of high-grade metamorphic rocks like khondalites, charnockites, and leptynites; (iii) sedimentary rocks of Paleozoic and Mesozoic age including limestones, sandstones, and conglomerates of Gondwana affinity; and (iv) extensive basaltic flows forming the Deccan Traps. Despite this complexity, the major contributors of sediments from the Peninsular region to the western Bay of Bengal can be grouped into two principal provenance zones: The Peninsular Granites and Gneisses (PGG) and the Deccan volcanic province. The PGG is mainly composed of ancient granitic and gneissic rocks, whereas the Deccan province represents extensive mafic lava flows (Goswami et al., 2012; Ahmad et al., 2009). The contrasting lithological and geochemical signatures of these two terrains allow for effective differentiation of their sedimentary inputs into the basin over geological timescales. Understanding the distinct provenance characteristics of these

source regions is critical for reconstructing past erosional and sedimentary patterns in the Bay of Bengal (Lupker et. al, 2013). In particular, tracing the relative contributions of the PGG and Deccan Traps to the basin can provide insights into how tectonic setting, lithology, and regional climate variability influence sediment delivery from the Indian Peninsula to marine depositional systems.

The Bay of Bengal (BoB) generally exhibits lower biological productivity in comparison to the Arabian Sea (AS), a difference largely attributed to the substantial freshwater input and resulting water column stratification. This stratification limits the upward transport of nutrient-rich deep waters to the sunlit surface layers where photosynthetic activity occurs (Prasanna Kumar et al., 2002). According to Verma et al. (2022), productivity levels in the BoB have fluctuated over time—being relatively higher during the last glacial period, when the Indian Summer Monsoon (ISM) was weak, and lower during the subsequent deglacial and Holocene periods, which were marked by a stronger ISM. The enhanced monsoonal activity during the deglacial and Holocene intervals led to increased freshwater discharge into the BoB, further intensifying stratification and thereby suppressing nutrient mixing into the photic zone. Conversely, during glacial phases when the ISM weakened, reduced stratification allowed for greater vertical mixing of the water column. During these periods, intensified north-easterly (NE) monsoon winds further facilitated the upward movement of nutrient-rich deeper waters, promoting enhanced productivity. Seasonal wind reversals also significantly influence BoB circulation patterns.

3 MATERIAL AND METHODS

3.1 Description of the Core

A piston core, VM29-19PC (R/V Vema, 1971) (14.71°N, 83.58°E), retrieved from the western Bay of Bengal (water depth ~ 3182 m) was investigated in this study (Fig. 1). The VM29-19PC core was archived at the LDEO (Lamont-Doherty Earth Observatory) Core Repository, Columbia University, USA and was subsampled at 2 cm interval (till 160 cm) and 1 cm interval (from 170 cm to 701 cm, except for 319.5 cm and 379.5 cm) for every 10 cm depth (not all) at LDEO, and a total of 57 samples were shipped to IISER Pune for geochemical analyses..

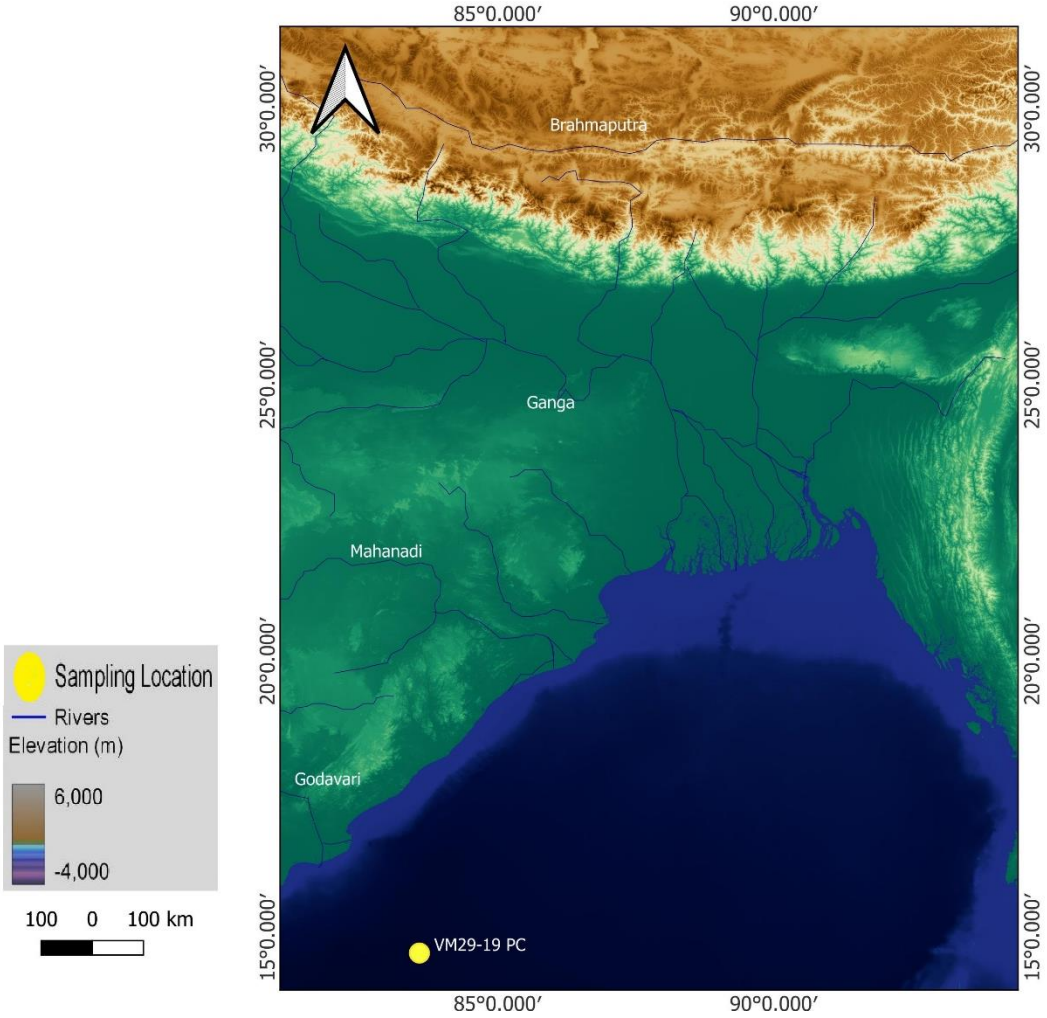

Figure 1: Location Map of the VM29-19 PC Sediment Core

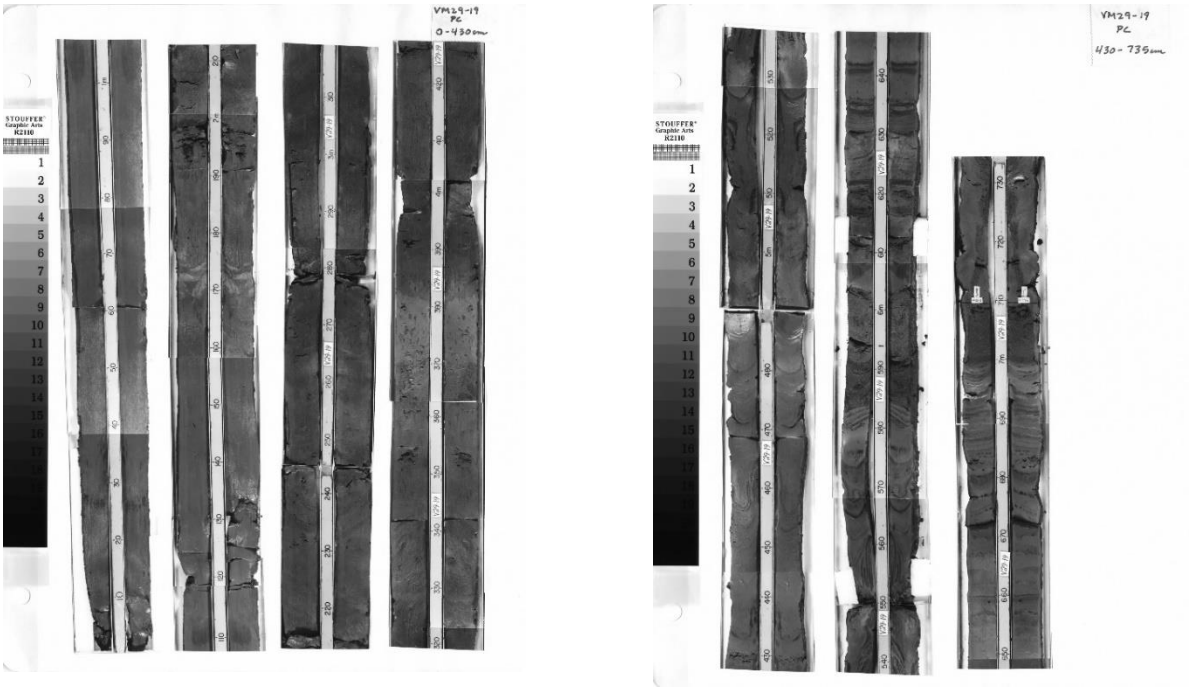

Figure 2: Picture of the VM29-19 PC sediment core (Picture Source: NOAA)

3.2 Chronology

The depth-age chronology for the core has already been established by Rashid et al. (2011). For this, 14C-AMS dates of mixed foraminifers from eight different depths between 106 and 296 cm were analyzed. These dates were calibrated to calendar years using the CALIB6.0.1 software (Reimer et al., 2009). Proper reservoir correction was applied during the calibration (Southon et al., 2002).

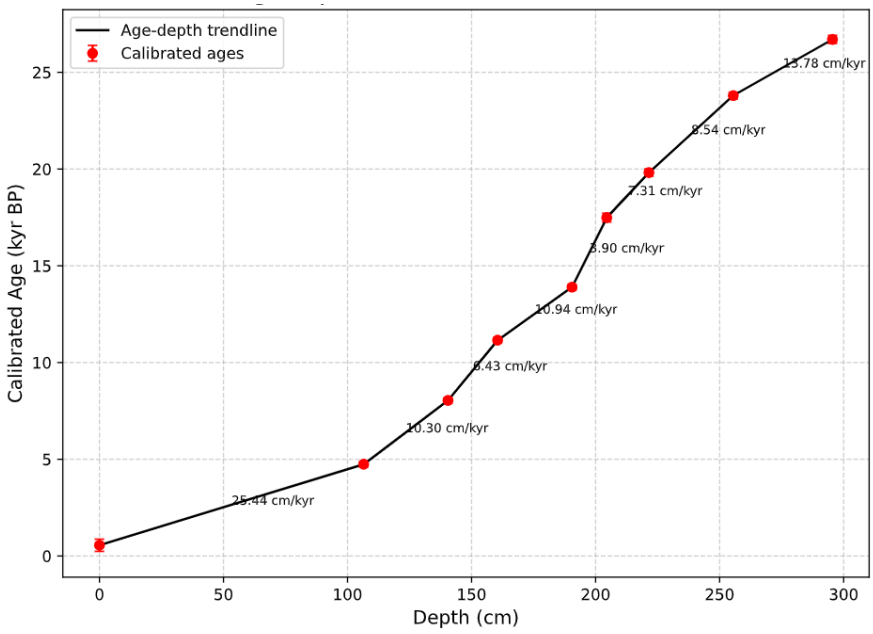

Figure 3: Age-depth relationship for the VM29-19 PC sediment core with sedimentation rates for the eight points

Existing radiocarbon dates, as reported by Rashid et al. (2011), serve as the basis for constructing an age-depth model using the Bchron method in R, which allows for Bayesian statistical modelling of radiocarbon-dated sequences. The age-depth relationship according to the 14C dating and Bchron model is shown in Fig. 3. The age of the surface (0 cm) has come approximately ~0.481 ka BP and at the 330 cm, it is 32.8 kyr BP. The sedimentation rates vary from 3.90 to 25.44 cm/ka, with an average of 10.83 cm/ka.

3.3 Geochemical Analyses

The geochemical procedures followed for analyzing the sediment core in this study were based on the protocols established by Tripathy et al. (2014). Approximately 5 grams of each sediment sample was first oven-dried at 60°C overnight to remove any residual moisture. After drying, the samples were ground manually using an agate mortar and pestle to obtain fine powders. These powdered samples were then rinsed thoroughly with deionized water to eliminate any residual marine salts. Following the washing process, the sediments were dried again and reground. These water-washed samples were used for subsequent geochemical measurement.

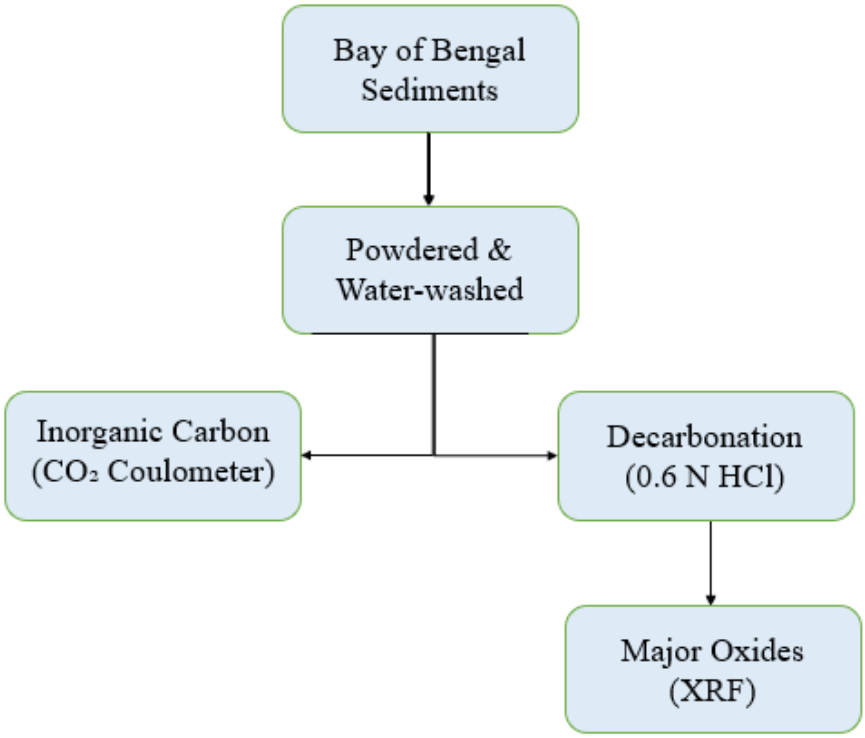

Figure 4: Flowchart of geochemical analyses adopted during this study

The water-washed samples were treated with 0.6 N HCl at 80°C to remove carbonate phases. During this process, the weight loss in sediments is used to compute the carbonate content. The analysis of major oxides was performed on the decarbonated fraction of the sediment samples. These aliquots were used for major oxide measurement using a X-Ray Fluorescence (XRF) spectrometer. For this, fusion bead of samples was prepared by mixing the sample with flux in 1:17 ratio. Each bead was produced by mixing roughly 0.55 grams of sediment with around 9.35 grams of a lithium metaborate/lithium tetraborate flux blend, along with a few drops of anhydrous lithium bromide as a releasing agent. Prior to fusion, the decarbonated samples were subjected to ignition at 950°C to determine the loss on ignition (LOI). The Bruker XRF system, calibrated with the GeoQuant Advance method, which yielded major oxide data with an accuracy of ±3% and a precision of ±5%. These concentrations data were used to calculate the Chemical Index of Alteration (CIA), a widely accepted proxy for assessing the intensity of chemical weathering in riverine systems, based on the equation established by Nesbitt and Young (1982).

$$CIA = \frac{Al_2O_3}{Al_2o_3 + Na_2O + K_2O + CaO^*} \times 100 \quad (1)$$

Here, the oxides concentrations are represented in molar units, and the term, CaO*, denotes the carbonate-corrected CaO of the sediment. A modified form, CIA*, has also been utilized to evaluate the degree of chemical weathering. The CIA* values are computed following the formula outlined by Tripathy et al. (2014).

$$CIA^* = \frac{Al_2O_3}{Al_2O_3 + Na_2O + K_2O} \times 100 \quad (2)$$

Table 1: Concentrations of major oxides for decarbonated fraction of sediment samples from the VM29-19 PC sediment core.

S. No.	Sample ID	Depth (cm)		LOI	Sum	Na_2O	MgO	Al_2O_3	SiO_2	P_2O_5	K_2O	CaO	TiO_2	Mn_2O_3	Fe_2O_3
		From	To	%											
1	19PC-01	0	2	15.4	94	0.46	1.86	15.14	48.15	0.10	1.83	0.39	1.16	0.06	8.18
2	19PC-02	10	12	16.3	93	0.52	1.57	14.37	48.72	0.09	1.76	0.45	1.17	0.06	7.39
3	19PC-03	18	20	15.1	99	0.35	1.91	16.01	51.58	0.11	1.81	0.26	1.24	0.08	9.14
4	19PC-04	30	32	17.7	98	0.26	1.76	15.81	50.10	0.11	1.74	0.16	1.12	0.06	8.66
5	19PC-05	40	41.5	17.0	100	0.26	1.81	16.39	51.31	0.12	1.82	0.17	1.12	0.06	8.99
6	19PC-06	50	52	16.7	98	0.26	1.65	16.24	51.12	0.11	1.91	0.16	1.07	0.06	8.29
7	19PC-07	60	62	16.0	99	0.29	1.74	16.74	51.79	0.11	1.98	0.15	1.04	0.07	8.41
8	19PC-08	68.5	70	16.9	98	0.30	1.72	16.44	51.05	0.10	1.98	0.14	1.01	0.06	8.03
9	19PC-09	81	82	15.2	99	0.32	1.73	16.76	53.27	0.10	2.15	0.17	1.04	0.07	7.84
10	19PC-10	89	90	17.4	98	0.30	1.62	16.17	51.18	0.09	2.08	0.14	0.98	0.06	7.47
11	19PC-12	110	111	17.1	98	0.36	1.85	16.17	50.76	0.10	2.26	0.20	0.95	0.06	7.44
12	19PC-14	129	131	13.9	99	0.33	1.71	17.30	53.97	0.10	2.34	0.18	1.00	0.07	7.77
13	19PC-15	140	141	16.4	97	0.34	1.60	16.36	50.92	0.09	2.14	0.18	0.92	0.06	7.30
14	19PC-16	150	151	16.8	94	0.37	1.67	15.70	48.50	0.09	2.07	0.18	0.86	0.06	7.46
15	19PC-17	158	160	15.0	98	0.55	1.67	15.63	53.56	0.09	2.37	0.29	0.99	0.07	7.21
16	19PC-18	170	171	15.4	95	0.84	1.83	14.53	51.05	0.08	2.24	0.64	0.94	0.06	6.50
17	19PC-19	181	182	15.4	98	0.53	1.93	15.96	52.84	0.09	2.31	0.30	0.97	0.06	7.14
18	19PC-20	190	191	13.8	98	0.63	2.12	15.72	54.23	0.09	2.45	0.35	0.98	0.07	7.02
19	19PC-22	210	211	14.0	99	0.81	2.00	15.25	55.41	0.08	2.57	0.45	0.97	0.07	6.34
20	19PC-23	219	220	12.7	97	0.82	2.33	16.18	53.54	0.09	2.62	0.45	0.92	0.09	6.42
21	19PC-24	229	232	14.1	95	0.78	2.24	15.28	51.48	0.08	2.51	0.44	0.89	0.10	6.65
22	19PC-25	240	241	14.3	95	0.77	1.92	15.29	52.42	0.08	2.46	0.38	0.93	0.06	6.09
23	19PC-26	250	251	13.0	96	0.86	2.38	15.69	52.62	0.08	2.57	0.52	0.96	0.07	6.41
24	19PC-27	260	261	13.4	97	0.86	2.31	15.78	53.01	0.08	2.58	0.49	0.93	0.06	6.60
25	19PC-29	279	281	13.0	98	0.74	1.98	15.48	55.71	0.08	2.57	0.38	0.92	0.08	6.67
26	19PC-30	290	291	9.1	90	0.78	1.88	14.83	52.37	0.08	2.45	0.38	0.90	0.06	6.33
27	19PC-31	300	301	9.6	93	0.67	2.22	15.62	52.75	0.09	2.43	0.36	0.94	0.07	7.08
28	19PC-33	319.5	321	14.8	97	0.76	2.20	16.09	52.01	0.09	2.58	0.42	0.87	0.09	6.84
29	19PC-34	330	331	14.3	98	0.85	1.76	16.37	53.75	0.08	2.74	0.43	0.89	0.08	5.75

4 RESULTS

The concentrations of elements such as Na (0.2–0.6, avg. 0.4 ± 0.30 wt%), Mg (0.9–1.4, avg. 1.1 ± 0.20 wt%), Al (7.6–9.2, avg. 8.4 ± 0.50 wt%), K (1.4–2.3, avg. 1.9 ± 0.30 wt%), Ti (0.5–0.7, avg. 0.6 ± 0.08 wt%), Fe (4.0–6.4, avg. 5.1 ± 0.96 wt%) exhibit noticeable variations across the sediment core. Table 2 compares these average elemental concentrations with their major sedimentary sources including the Ganga-Brahmaputra (Garzanti et al., 2011), Godavari-Krishna (Pattan et al., 2008), and Mahanadi Rivers (Bastia et al., 2019, Lee et. al, 2022). Most of the elemental abundances, with the exception of Al and Ca, overlap with the expected source composition. This mismatch may arise from the difference in mobility of these elements (for Al), or, its uptake during biological/authigenic processes (for Ca).

Table 2: Average major compositions of the VM29-19 PC core are compared with those reported for the major sedimentary sources (Data source: Tripathy et al., 2014; Bastia et al., 2019)

Wt%	Ganga	Brahmaputra	Godavari-Krishna	Mahanadi	VM29-19 PC
Na	0.7	1.3	0.6	0.7	0.7
Mg	1.5	1.6	1.5	0.2	1.1
Al	7.9	8.0	8.0	5.2	8.4
K	2.3	2.6	1.7	3.8	0.3
Ca	2.1	1.4	2.0	0.8	0.4
Ti	0.5	0.4	0.8	0.2	0.5
Fe	4.6	4.1	6.4	2.7	4.2
CIA*	77	71	81	60	82

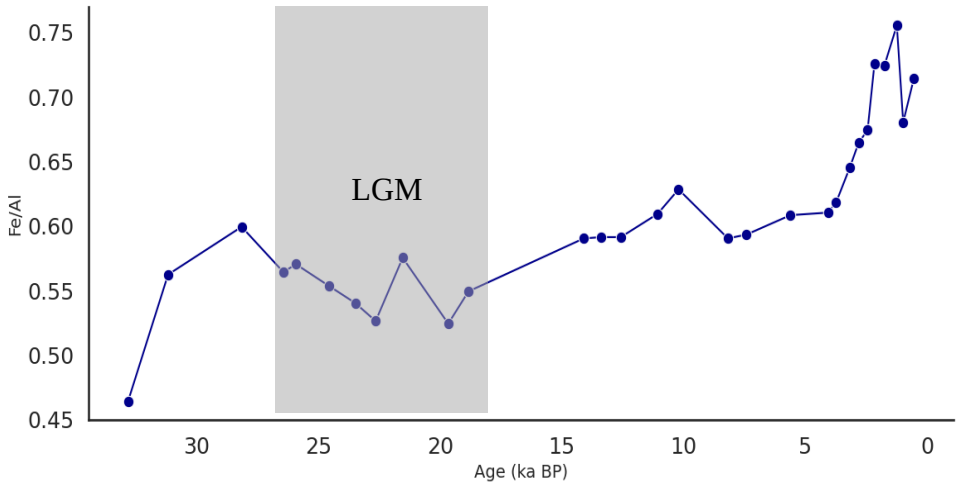

Figure 5: Down-core variation in Al normalized ratio of Fe

The CIA and CIA* values vary between 80 and 88 (avg. 84 ± 2, n=29) and 82 and 89 (avg. 85 ± 3, n=29), respectively. A systematically lower CIA values were observed for younger (than ~ 12 ka) samples falling from 88 to 80 (Fig. 6). Additionally, the K/Al and Ti/Al also show significant temporal changes over the past ~33 ka.

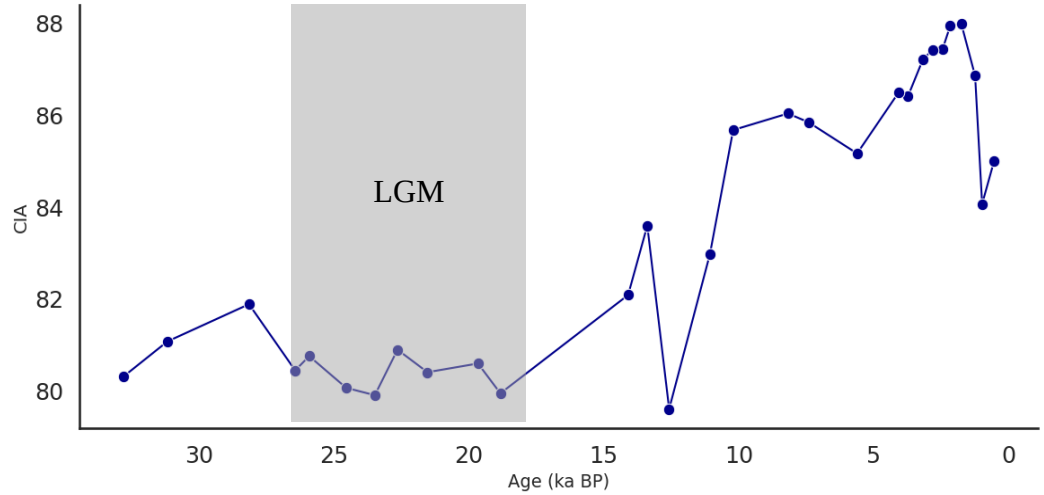

Figure 6: Trend of CIA is shown with respect to Age (ka BP)

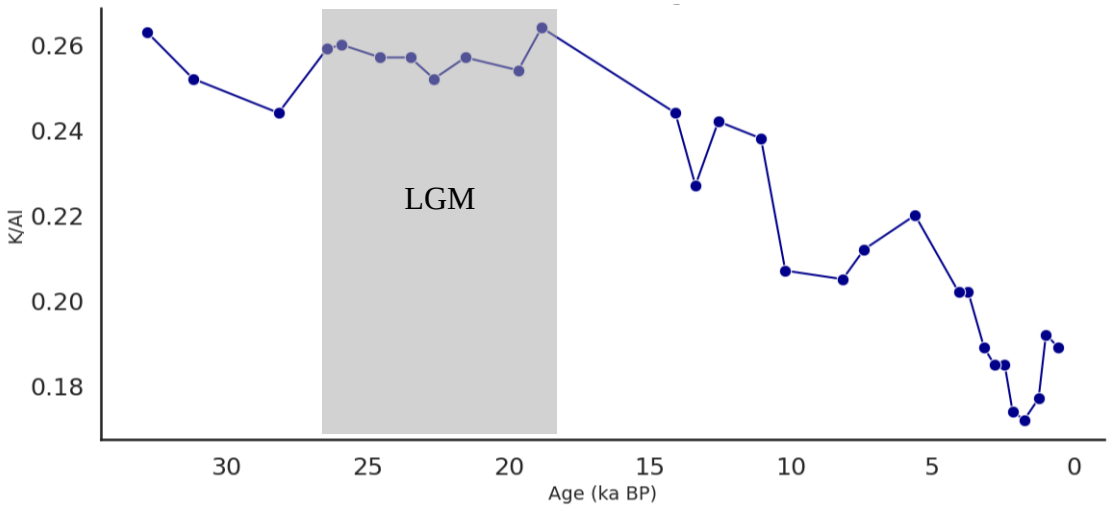

Figure 7: Trend of K/Al is shown with respect to Age (ka BP)

5 DISCUSSION

Chemistry of oceanic sediments, in their decarbonated fractions, reflects relative contribution of sedimentary sources and relative mobility of elements during chemical weathering on land. The Ti/Al ratio, often used as a tracer for detrital provenance, remains relatively stable throughout the core but shows subtle fluctuations (Fig. 8). Higher values in the early Holocene (~0–5 ka BP) and during 13–26 ka BP suggest an enhanced contribution of mafic minerals, possibly from the Deccan Traps or Peninsular India sources (Tripathy et al., 2011; France-Lanord et al., 1993). These intervals correspond with the periods of higher Fe/Al ratios observed earlier in your data and imply that sediment flux from southern catchments increased during periods of weakened monsoon when the Himalayan rivers carried less load. Lower Ti/Al values during mid-Holocene (~5–10 ka BP) could reflect a relatively stronger Himalayan input dominated by felsic lithologies with lower Ti content. This is consistent with higher CIA values during this time, indicating intense weathering of silicate-rich Himalayan rocks under strengthened monsoon conditions.

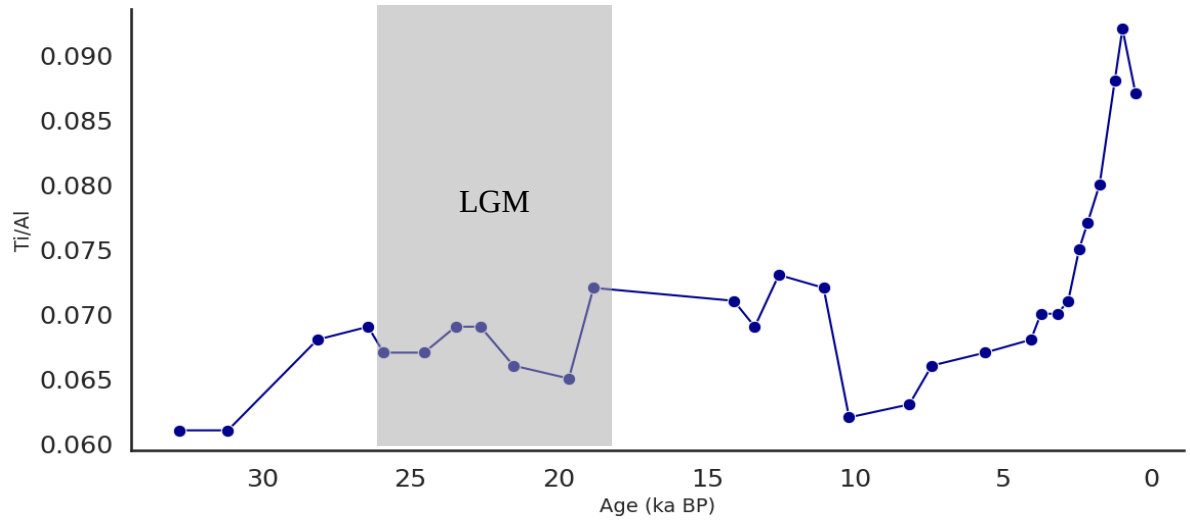

Figure 8: Trend of Ti/Al is shown with respect to Age (ka BP)

The correlation matrix (Table 2) of the major oxides in the VM29-19 PC sediment core reveals important geochemical associations that shed light on elemental behavior and possible sediment sources. A notably strong positive correlation is observed between Al and Fe, suggesting a common detrital origin, likely associated with aluminosilicate minerals such as clays and iron-bearing silicates. This relationship indicates that both aluminum and iron are

predominantly derived from terrestrial sources and likely remain immobile during early diagenesis. The alkali elements, K and Na, both show a good positive correlation with Al, further supporting their incorporation in clay minerals such as illite or feldspars.

Table 3: Correlation matrix of the major elemental data of the VM29-19 PC sediment core.

	Na	K	Ca	Mg	Al	Fe	Ti
Na	1						
K	0.82	1					
Ca	0.92	0.57	1				
Mg	0.70	0.64	0.62	1			
Al	-0.53	-0.05	-0.68	-0.16	1		
Fe	-0.88	-0.87	-0.72	-0.45	0.39	1	
Ti	-0.58	-0.80	-0.32	-0.35	0.04	0.79	1

The relationship between K and Na themselves is also strong, indicating similar source contributions or shared mineral hosts. This pattern reflects weathering of continental rocks, where these elements are typically associated with primary silicates and are retained in the fine fraction of sediments. CaO, on the other hand, shows a generally weak correlation with the other major oxides. This suggests that calcium may have a more varied origin, possibly influenced by biogenic carbonates or fluctuating marine productivity, and may not be entirely linked to the terrigenous detrital fraction. MgO shows moderate positive correlations with both Al and Fe, which could indicate partial association with clay minerals or ferro-magnesian silicates derived from mafic source rocks. This relationship may also point to a mixed origin, where magnesium exists in both detrital and authigenic phases. Si shows a moderate to strong negative correlation with Al and Fe, a pattern that is often observed in sediment cores where quartz dilution plays a role (Lupker et al., 2013). Since quartz is rich in silica but poor in other elements, its abundance tends to dilute concentrations of more chemically active components. This negative association supports the idea that variations in Si may largely reflect fluctuating inputs of quartz-rich materials versus finer, clay-dominated sediments. Overall, the correlation matrix supports the interpretation that much of the sediment composition in the VM29-19 PC core is controlled by terrestrial input dominated by clay minerals and silicate weathering products, with some influence from biogenic or marine-derived components, particularly for calcium.

In addition to these phase changes, the elemental changes may also be linked to relative mobility of elements during chemical weathering processes. To evaluate the relative depletion

or enrichment of potassium during chemical weathering, we adopted an aluminum-normalized approach for calculating the K/Si* index following the method outlined by Lupker et al. (2013). This method uses the strong correlation between Al/Si and K/Si in detrital source material to establish a baseline against which deviations in the sediment core can be interpreted. The relationship is expressed as:

$$\frac{K^*}{Si} = \frac{Al}{Si} \times A + B \tag{3}$$

where A = 0.23 is the empirically determined slope derived from typical detrital inputs (Lupker et al., 2013), and B is the y-intercept computed from linear regression of the dataset. In this study, we used this formulation to define the expected detrital trend of K/Si as a function of Al/Si. Any sample that plots (Fig. 9) below the calculated regression line suggests a depletion in potassium relative to its aluminum and silicon content, typically due to leaching during chemical weathering. Conversely, points on or above the trend line indicate minimal chemical alteration. This approach allows for a more accurate assessment of weathering intensity over time by filtering out the effects of mineralogical sorting and grain size variability, particularly valuable in the context of sediment cores from dynamic depositional settings like the Bay of Bengal.

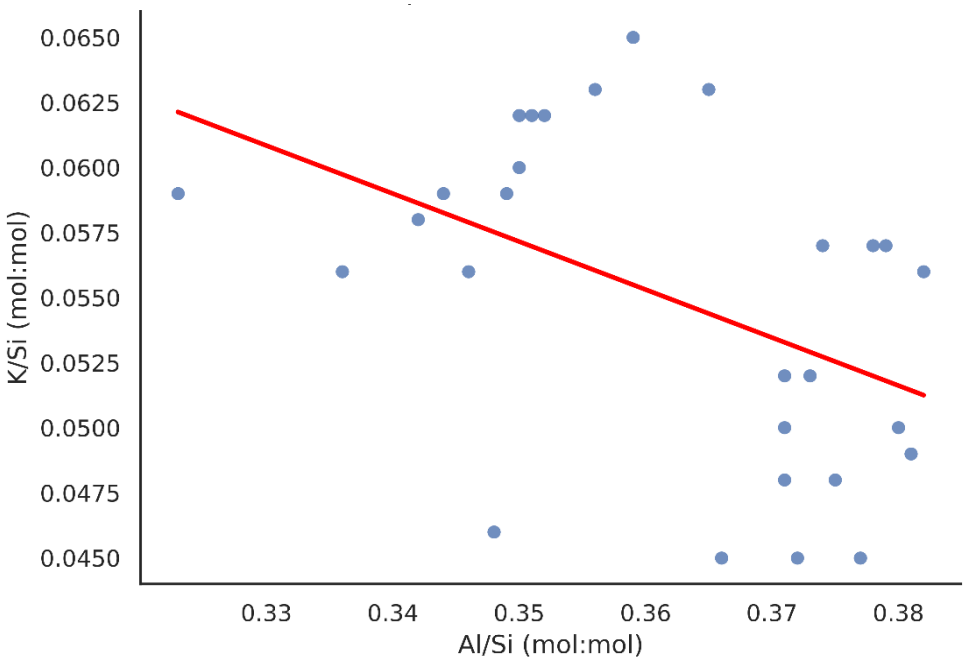

Figure 9: Correlation between K/Si and Al/Si

5.1 Potassium to Aluminium Ratio (K/Al)

The K/Al ratio, which is considered a sensitive indicator of the intensity of chemical weathering (especially leaching of mobile elements like K), shows a gradual increasing trend from the LGM to the Holocene (Fig. 7). Lower K/Al values (~0.18–0.20) during the LGM suggest higher degrees of leaching and stronger weathering of feldspar minerals, despite the overall low CIA. This may seem contradictory, but it aligns with the fact that Al tends to be retained even during intense weathering, while K is more mobile (Nesbitt et al., 1996). Post-LGM, K/Al increases steadily, indicating a relative decrease in weathering intensity or possibly a shift in sediment provenance (Peketi et. al, 2020, 2021). The K/Al ratio stabilizes during the mid to late Holocene, supporting the idea of climatic stabilization and consistent sediment delivery, potentially from the Peninsular rivers like the Godavari and Krishna (Pattan et al., 2008; Tripathy et al., 2011). Interestingly, the drop in K/Al ratio around 5 ka could correspond to a short-wet phase, possibly related to intensified monsoonal rainfall, causing enhanced chemical leaching of K relative to Al (Sinha et al., 2005).

5.2 Chemical Index of Alteration (CIA) Trends

The Chemical Index of Alteration (CIA), a widely accepted proxy for chemical weathering intensity, shows a distinct temporal evolution through the last ~33 ka (Fig. 6). The CIA values in the core fluctuate between ~80 and 89, indicating varying degrees of chemical weathering in the sediment source regions, primarily the Himalayan and Peninsular India river basins (Nesbitt and Young, 1982; Tripathy et al., 2011). A key observation is the gradual increase in CIA values from ~26 ka to the present, reflecting intensified chemical weathering over time. This trend correlates well with the global deglacial warming and increased monsoonal activity after the Last Glacial Maximum (LGM; ~21 ka BP) (Peterson et al., 2000; Galy and France-Lanord, 2001). During the LGM, CIA values are relatively low (~80–83), which is consistent with the colder, drier climate conditions that prevailed across South Asia and the reduced intensity of the Indian summer monsoon (Tiwari et al., 2010). Such conditions suppressed chemical weathering in the Himalayan catchments. Following the LGM, the steady rise in CIA values suggests enhanced silicate weathering, likely due to stronger summer monsoon rainfall and warmer temperatures during the Holocene. Notably, the CIA reaches a peak (~88) around 3–5 ka BP, coinciding with the Holocene Climatic Optimum, a period of intensified monsoon and elevated precipitation (Gupta et al., 2003). A temporary dip in CIA around 13–14 ka BP might reflect the Younger Dryas (YD) event (~12.9– 11.7 ka BP), a well-documented short

cold reversal during the deglaciation. This abrupt cooling event led to reduced monsoon strength and hence diminished chemical weathering (Alley, 2000; Tiwari et al., 2010). This climatic signal is echoed in the sharp decline in CIA values around that period. The overall increase of CIA after ~13 ka may be the result of various sources of the sediments as apart from the Himalayas, the Bay of Bengal also consist sediments of Deccan plateau. So, the increase does not only reflect its linkage to weathering but also suggest sediment provenance. So, isotopic studies, e.g. Sr-Nd may infer the trend better which may be a part of the future study.

5.3 Weathering and Climate interaction

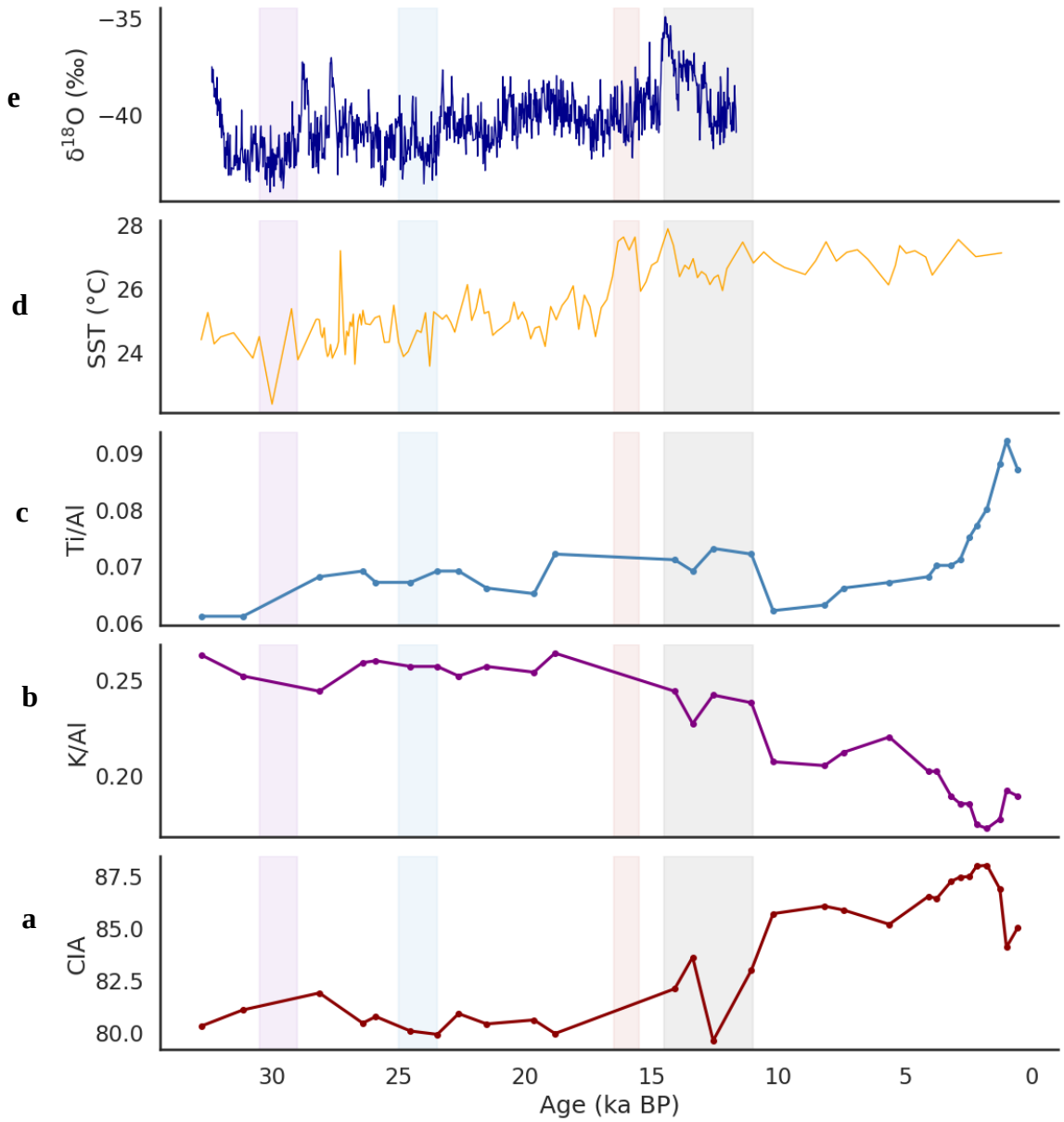

Figure 10: Depth profiles of weathering indices a) CIA, b) K/Al, c) Ti/Al of VM29-19 PC compared with climatic indicators d) SST (°C) with Age (ka BP) of core BoB-24 (Liu et al., 2021)) and e) $\delta^{18}O$ (SMOW) with Age (ka BP) of GISP-2 ice core from Greenland (Andersen et al., 2006)

The above discussion clearly highlights several significant climatic transitions:

- **Last Glacial Maximum (~26–21 kyr BP)**: Characterized by relatively low CIA and low K/Al, reflecting subdued weathering due to arid and cold conditions (Galy and France-Lanord, 2001). Provenance signals suggest enhanced input from Peninsular sources.
- **Deglaciation Phase (21–11 kyr BP)**: Marked by a gradual rise in CIA and K/Al ratios. The period around 13–14 kyr BP shows a sharp drop in CIA, possibly representing the **Younger Dryas**, a return to cold conditions before the full onset of the Holocene.
- **Early Holocene (~11–8 kyr BP)**: A phase of increased CIA and K/Al, reflecting intensified chemical weathering driven by warmer and wetter climate. This aligns with the **Holocene Climatic Optimum**, a period of stronger ISM activity (Gupta et al., 2003; Dutt et al., 2015).
- **Mid to Late Holocene (~8–0 kyr BP)**: CIA values remain elevated with minor fluctuations, indicating relatively stable climatic conditions. A brief dip in K/Al around 5 kyr may point to a short-lived humid event.

During the LGM, reduced CIA values reflect the widespread glacial and periglacial conditions in the Himalayas, suppressing chemical weathering (Lambeck et. al, 2014). Instead, mechanical weathering likely dominated, resulting in the transport of less-altered minerals downstream (Galy and France- Lanord, 2001). The cold, dry conditions curtailed silicate breakdown, as evidenced by the consistently lower chemical indices. This contrasts with the Holocene period, where intensification of the monsoon promoted chemical alteration of silicate rocks in the Himalayan foothills and Ganga-Brahmaputra plains, enhancing the CIA values. The Chemical Index of Alteration (CIA) profile generated from our sediment core analysis reveals significant temporal variability that appears to correspond with independent paleoclimatic proxies from previously published studies (Fig. 10). Notably, the CIA values display a declining trend through time, with intermittent fluctuations that may be interpreted as responses to shifts in monsoonal intensity and weathering processes. the comparison with $\delta^{18}O$ records from the North Greenland Ice Core Project (NGRIP) (Andersen et al., 2006) is also shown, which indicate Northern Hemisphere climatic variability. the $\delta^{18}O$ values represent various shifts in ice volume and temperature, which align with the overall trend of CIA. For instance, CIA maxima tend to align with lower $\delta^{18}O$ values, which are associated with colder and presumably wetter periods, conducive to enhanced chemical alteration of silicate minerals.

This convergence across disparate proxies—CIA from sediment geochemistry, SST from marine records, and $\delta^{18}O$ from ice cores—underscores the robustness of the observed paleoenvironmental trends. Such multi-proxy agreement strengthens the interpretation that the CIA variations documented in this study are reflective of regional and hemispheric climate fluctuations over the timescales represented in the core. When compared against Sea Surface Temperature (SST) reconstructions from the Bay of Bengal by Liu et al. (2021), a coherent pattern emerges. Periods of lower CIA values tend to align with warmer SST phases, suggesting a possible weakening of chemical weathering during warmer climatic intervals, potentially linked to reduced precipitation or runoff. In contrast, the high values of CIA more or less refer to cooler SST regime, which indicates the intensification of weathering under the influence of very strong monsoonal phase.

6 CONCLUSIONS

This study reconstructs past erosional pattern over the Himalayan (and peninsular Indian) river basins during the last ~33,000 years through detailed geochemical analysis of theBay of Bengal sediments. It establishes strong climate and weathering coupling by examining chemical weathering proxies such as the Chemical Index of Alteration (CIA), K/Al, and Ti/Al ratios. The CIA values reveal a progressive increase in chemical weathering intensity from the Last Glacial Maximum (LGM) through the Holocene. Lower CIA values during the LGM indicate subdued chemical alteration in sediment source regions, likely caused by colder and drier climatic conditions. The steady rise of the CIA values throughout the Early and Mid- Holocene points to effect of monsoon intensification on weathering intensity. The K/Al ratio shows mobility of potassium under various weathering conditions. The increase of the K/Al ratio from the glacial to the interglacial period is attributable to elemental mobility during chemical weathering and/or sediment provenance change. During Early Holocene, the K/Al ratio variations may indicate enhanced chemical weathering under higher degree of monsoon. Whereas, Ti/Al ratio stays more or less stable, showing minute fluctuations which may suggest to different contributions of sediment from both the Himalayan and Peninsula India.. There are some climatic events which existed for a short amount of time in the past geologic time, e.g. Younger Dryas, Holocene wet phases which are identifiable by sudden changes in K/Al ratio and CIA. This study focuses on various geochemical proxies which shed light on the links between glacial-interglacial cycles and chemical weathering in South Asia. It has shown the connections between the supply of sediments and various climatic changes, which also explains the importance of ISM and Himalayan orogeny. These have played a crucial role in making the sedimentary and geochemical evolution of Bay of Bengal. This study also indicates that how minute changes in monsoon can affect overall chemical weathering over millennial timescales.

7 REFERENCES

Ahmad, S.M., Padmakumari, V.M. and Babu, G.A., 2009. Strontium and neodymium isotopic compositions in sediments from Godavari, Krishna and Pennar rivers. *Current science*, pp.1766-1769.

Bastia, F., Equeenuddin, S.M., Roy, P.D. and Hernández-Mendiola, E., 2020. Geochemical signatures of surface sediments from the Mahanadi river basin (India): Chemical weathering, provenance, and tectonic settings. Geological Journal, 55(7), pp.5294-5307.

Bluth, G.J. and Kump, L.R., 1994. Lithologic and climatologic controls of river chemistry. *Geochimica et Cosmochimica Acta*, *58*(10), pp.2341-2359.

Cai, M., Xu, Z., Clift, P.D., Lim, D., Khim, B.K., Yu, Z., Kulhanek, D.K., Li, T., Chen, H. and Sun, R., 2019. Depositional history and Indian summer monsoon controls on the silicate weathering of sediment transported to the eastern Arabian Sea: Geochemical records from IODP Site U1456 since 3.8 Ma. *Geochemistry, Geophysics, Geosystems*, *20*(9), pp.4336-4353.

France-Lanord, C. and Derry, L.A., 1997. Organic carbon burial forcing of the carbon cycle from Himalayan erosion. *Nature*, *390*(6655), pp.65-67.

Galy, V., François, L., France-Lanord, C., Faure, P., Kudrass, H., Palhol, F. and Singh, S.K., 2008. C4 plants decline in the Himalayan basin since the Last Glacial Maximum. Quaternary Science Reviews, 27(13-14), pp.1396-1409.

Garzanti, E., Andó, S., France-Lanord, C., Censi, P., Vignola, P., Galy, V. and Lupker, M., 2011. Mineralogical and chemical variability of fluvial sediments 2. Suspended-load silt (Ganga–Brahmaputra, Bangladesh). *Earth and Planetary Science Letters*, *302*(1-2), pp.107-120.

Goodbred Jr, S.L. and Kuehl, S.A., 2000. Enormous Ganges-Brahmaputra sediment discharge during strengthened early Holocene monsoon. *Geology*, *28*(12), pp.1083-1086.

Goswami, V., Singh, S.K., Bhushan, R. and Rai, V.K., 2012. Temporal variations in 87Sr/86Sr and ε_{Nd} in sediments of the southeastern Arabian Sea: Impact of monsoon and surface water circulation. *Geochemistry, Geophysics, Geosystems*, *13*(1).

Hilton, R.G. and West, A.J., 2020. Mountains, erosion and the carbon cycle. *Nature Reviews Earth & Environment*, *1*(6), pp.284-299.

Lambeck, K., Rouby, H., Purcell, A., Sun, Y. and Sambridge, M., 2014. Sea level and global ice volumes from the Last Glacial Maximum to the Holocene. *Proceedings of the National Academy of Sciences*, *111*(43), pp.15296-15303.

Lee, J., Kim, S., Ikehara, M., Horikawa, K., Asahara, Y., Yoo, C.M. and Khim, B.K., 2022. Indian monsoon variability in the Mahanadi Basin over the last two glacial cycles and its implications on the Indonesian throughflow. Geoscience Frontiers, p.101483.

Lupker, M., France-Lanord, C., Galy, V., Lavé, J. and Kudrass, H., 2013. Increasing chemical weathering in the Himalayan system since the Last Glacial Maximum. Earth and Planetary Science Letters, 365, pp.243-252.

Mandal, S.K., Lupker, M., Burg, J.P., Valla, P.G., Haghipour, N. and Christl, M., 2015. Spatial variability of 10Be-derived erosion rates across the southern Peninsular Indian escarpment: A key to landscape evolution across passive margins. *Earth and Planetary Science Letters*, *425*, pp.154-167.

Milliman, J.D. and Syvitski, J.P., 1992. Geomorphic/tectonic control of sediment discharge to the ocean: the importance of small mountainous rivers. *The journal of Geology*, *100*(5), pp.525-544.

Mohanty, P.K., Pradhan, Y., Nayak, S.R., Panda, U.S. and Mohapatra, G.N., 2008. Sediment dispersion in the Bay of Bengal. *Monitoring and modelling lakes and coastal environments*, pp.50-78.

Naidu, P.D. and Govil, P., 2010. New evidence on the sequence of deglacial warming in the tropical Indian Ocean. Journal of Quaternary Science, 25(7), pp.1138-1143.

Nesbitt, H. and Young, G.M., 1982. Early Proterozoic climates and plate motions inferred from major element chemistry of lutites. nature, 299(5885), pp.715-717.

Pattan, J.N., Pratibhan, G., Babu, C.P., Khadge, N.H., Paropkari, A.L. and Kodagali, V.N., 2008. A note on geochemistry of surface sediments from Krishna-Godavari basin, East Coast of India. *Geological Society of India*, *71*(1), pp.107-114.

Peketi, A., Mazumdar, A., Pillutla, S.P.K., Rai, V.K., Sawant, B. and Chaitanya, A.V.S., 2020. Monsoon rainfall and contrasting source rocks influenced sediment composition of peninsular basins along the east coast of India (western Bay of Bengal). Marine and Petroleum Geology, 118, p.104433.

Peketi, A., Mazumdar, A., Pillutla, S.P.K., Sawant, B. and Gupta, H., 2021. Climatic and tectonic control on the Bengal fan sedimentation since the Pliocene. Geochemistry, Geophysics, Geosystems, 22(3), p.e2020GC009448.

Prasanna Kumar, S., Muraleedharan, P.M., Prasad, T.G., Gauns, M., Ramaiah, N., De Souza, S.N., Sardesai, S. and Madhupratap, M., 2002. Why is the Bay of Bengal less productive during summer monsoon compared to the Arabian Sea. *Geophysical Research Letters*, *29*(24), pp.88-1.

Rahaman, W., Singh, S.K., Sinha, R. and Tandon, S.K., 2009. Climate control on erosion distribution over the Himalaya during the past~ 100 ka. *Geology*, *37*(6), pp.559-562.

Raymo, M.E. and Ruddiman, W.F., 1992. Tectonic forcing of late Cenozoic climate. *Nature*, *359*(6391), pp.117-122.

Samanta, A., Tripathy, G.R., Nath, B.N., Bhushan, R., Panchang, R., Bharti, N. and Shrivastava, A., 2022. Holocene variability in chemical weathering and ocean redox state: A reconstruction using sediment geochemistry of the Arabian Sea. *Journal of Asian Earth Sciences*, *224*, p.105029.

Sengupta, D., Bharath Raj, G.N. and Shenoi, S.S.C., 2006. Surface freshwater from Bay of Bengal runoff and Indonesian throughflow in the tropical Indian Ocean. *Geophysical Research Letters*, *33*(22).

Singh, S.K., Rai, S.K. and Krishnaswami, S., 2008. Sr and Nd isotopes in river sediments from the Ganga Basin: sediment provenance and spatial variability in physical erosion. *Journal of Geophysical Research: Earth Surface*, *113*(F3).

Tripathy, G.R., Singh, S.K., Bhushan, R. and Ramaswamy, V., 2011. Sr–Nd isotope composition of the Bay of Bengal sediments: impact of climate on erosion in the Himalaya. Geochemical Journal, 45(3), pp.175-186.

Tripathy, G.R., Singh, S.K. and Ramaswamy, V., 2014. Major and trace element geochemistry of Bay of Bengal sediments: Implications to provenances and their controlling factors. *Palaeogeography, Palaeoclimatology, Palaeoecology*, *397*, pp.20-30.

Verma, K., Singh, A.D., Singh, P., Singh, H., Satpathy, R.K., Uddandam, P.R. and Naidu, P.D., 2022. Monsoon-related changes in surface hydrography and productivity in the Bay of Bengal over the last 45 kyr BP. *Palaeogeography, Palaeoclimatology, Palaeoecology*, *589*, p.110844.

Von Blanckenburg, F., Bouchez, J., Ibarra, D.E. and Maher, K., 2015. Stable runoff and weathering fluxes into the oceans over Quaternary climate cycles. *Nature Geoscience*, *8*(7), pp.538-542.

White, A.F., Blum, A.E., Bullen, T.D., Vivit, D.V., Schulz, M. and Fitzpatrick, J., 1999. The effect of temperature on experimental and natural chemical weathering rates of granitoid rocks. *Geochimica et Cosmochimica Acta*, *63*(19-20), pp.3277-3291.